

Intrinsic Correlations for Flaring Blazars Detected by Fermi

J. H. Fan^{1,2},¹ J. H. Yang^{3,2}, H. B. Xiao^{1,2}, C. Lin^{1,2}, D. Constantin^{1,2}, G. Y. Luo^{1,2}, Z.Y. Pei^{1,2}, J. M. Hao^{1,2}, Y. W. Mao^{1,2}

1. *Center for Astrophysics, Guangzhou University, Guangzhou 510006, China*

2. *Astronomy Science and Technology Research Laboratory of Department of Education of Guangdong Province, Guangzhou 510006, China*

3. *Department of Physics and Electronics Science, Hunan University of Arts and Science, Changde 415000, China*

ABSTRACT

Blazars are an extreme subclass of active galactic nuclei. Their rapid variability, luminous brightness, superluminal motion, and high and variable polarization are probably due to a beaming effect. However, this beaming factor (or Doppler factor) is very difficult to measure. Currently, a good way to estimate it is to use the time scale of their radio flares. In this *Letter*, we use multiwavelength data and Doppler factors reported in the literatures for a sample of 86 flaring blazars detected by Fermi to compute their intrinsic multiwavelength data and intrinsic spectral energy distributions, and investigate the correlations among observed and intrinsic data. Quite interestingly, intrinsic data show a positive correlation between luminosity and peak frequency, in contrast with the behavior of observed data, and a tighter correlation between γ -ray luminosity and the lower energy ones. For flaring blazars detected by Fermi, we conclude that (1) Observed emissions are strongly beamed; (2) The anti-correlation between luminosity and peak frequency from the observed data is an apparent result, the correlation between intrinsic data being positive; and (3) Intrinsic γ -ray luminosity is strongly correlated with other intrinsic luminosities.

Subject headings: Active galactic nuclei: general, galaxies: active, galaxies: jets, galaxies: nuclei

Supporting material: data behind figures, machine-readable table

¹email:fjh@gzhu.edu.cn

²email:yjianghe@163.com

1. Introduction

Blazars show extreme observational properties (Acero et al. 2015; Ackermann et al. 2015; Fan et al. 2016a,b; and reference therein). They are divided into two main subclasses, BL Lacertae objects (BL Lacs) and flat spectrum radio quasars (FSRQs), following to the behavior of their emission lines and further subdivided according to their synchrotron peak frequency (Padovani & Giommi 1995; Nieppola et al. 2006; Abdo et al. 2010; Fan et al. 2016a,c). Recently, Massaro et al. (2015) published the largest blazar sample (the BZCAT 5.0 (<http://www.asdc.asi.it/bzcat/>)).

Blazars were detected by EGRET (Hartman et al. 1999) and are the main discovery of Fermi/LAT mission (Abdo et al. 2009; Nolan et al. 2012; Acero et al. 2015; Ackermann et al. 2015). The correlation between γ -rays and radio bands suggests a strong beaming effect in γ -rays (Dondi & Ghisellini 1995; Fan et al. 1998; Huang et al. 1999; Cheng et al. 2000; Fan et al. 2016a), and the beaming factors (or Doppler factors) are estimated for some γ -ray loud blazars based on their rapid γ -ray variability time scale, X-ray and γ -ray emissions (Mattox et al. 1993, von Montigny et al. 1995, Cheng, et al. 1999; Fan et al. 1999; 2009; 2013; 2014; Fan 2005). In addition, a useful method to estimate Doppler factors may be found in a work (Lähteenimäki & Valtaoja 1999), followed by many other works (Fan et al. 2009; Hovatta et al. 2009; Lister et al. 2009a; Savolainen et al. 2010). Doppler factor is also obtained by a synchrotron self-Compton mechanism (Ghisellini et al. 1993).

The strong beaming effect could be the reason of the correlations among different energy bands and among the observed parameters. For this reason, we investigate whether such correlations hold even for the intrinsic emission. We adopt $f^{in} = f^{ob}/\delta^p$, where f^{in} is the intrinsic (or de-beamed) flux density, f^{ob} is the observed flux density, δ is a Doppler factor (or boosting factor), $p = 2 + \alpha$ for a continuous jet (or $p = 3 + \alpha$ for a spherical jet), and α is a spectral index ($f_\nu \propto \nu^{-\alpha}$).

In this *Letter* we investigate the relationship between the observed γ -ray luminosity and the peak frequency and those among their intrinsic values for a sample of Fermi blazars (Fan et al. 2016a) with available Doppler factors. The sample properties are presented in section 2, the results in section 3 while in section 4 we give our conclusions.

2. Sample and Results

In this *Letter*, a sample of 86 flaring blazars detected by Fermi (55 FSRQs and 31 BLs) with available Doppler factor (Lähteenimäki & Valtaoja 1999; Fan et al. 2009; Hovatta et al. 2009; Lister et al. 2009a; Savolainen et al. 2010) is compiled. Their synchrotron peak fre-

quency, multi-wavelength monochromatic luminosity, and peak luminosity are from our recent paper (Fan et al. 2016a). The radio data is at 1.4 GHz, optical data at R band, and the X-ray data at 1 KeV. But the X-ray flux density is only available for 82 sources, the corresponding multiwavelength luminosities are shown in Table 3.

For the sample, we investigate the relationship between luminosity and Doppler factor and show the results in Table 2 and Fig. 1. For the relationship between the peak frequency, $\log\nu$, and luminosity, the corresponding results are listed in Table 2 and shown in Fig. 2.

When we consider the intrinsic (or de-beamed) monochromatic luminosity, we have $\log(\nu L_\nu^{\text{in}}) = \log(\nu L_\nu) - (p + 1) \log\delta$. Here we obtain the spectral index, α by fitting the data ($f_\nu \propto \nu^{-\alpha}$) at the corresponding bands. We calculate radio spectral indexes (α_R) for all the 86 sources, optical indexes (α_O) for 62 sources, and X-ray spectral indexes (α_X) for only 5 sources. For the sources without fitting α_O and α_X , we look for those parameters from the available literatures and get 70 α_X 's and 4 α_O 's. Then we have averaged spectral index, $\langle \alpha_O \rangle = 1.155$ for 28 BL Lacs and $\langle \alpha_O \rangle = 0.805$ for 38 FSRQs; $\langle \alpha_X \rangle = 1.021$ for 25 BL Lacs and $\langle \alpha_X \rangle = 0.738$ for 50 FSRQs, they are used to replace unknown spectral indexes.

For the intrinsic peak frequency, peak flux, and integrated flux, we use the intrinsic multiwavelength data to calculate the SEDs as did in Fan et al. (2016a), $\log(\nu^{\text{in}} f_\nu^{\text{in}}) = -P_1(\log\nu^{\text{in}} - P_2)^2 + P_3$, here $f^{\text{in}} = f^{\text{ob}}/\delta^p$, $\nu^{\text{in}} = \nu/(\delta/(1+z))$, P_1 is a curvature parameter, P_2 is the intrinsic peak frequency, and P_3 is the intrinsic integrated flux, from which we calculate the intrinsic bolometric luminosity.

The correlation between intrinsic γ -luminosity and monochromatic (peak and bolometric) luminosity are shown in Fig. 1 and those between the intrinsic luminosity and peak frequency are listed in Table 2 and shown in Fig. 2.

3. Discussions

AGNs are the most numerous population of detected sources in the Fermi mission, which provide us with a good opportunity to study their emission mechanism and beaming effects.

In 1998, Fossati, et al. calculated the spectral energy distribution for a sample of blazars (RBLs, XBLs, and FSRQs), investigated the relationship between the radio luminosity (peak luminosity) and peak frequency, and found that there is a sequence for blazars with higher radio luminosity sources corresponding to lower frequency and lower luminosity sources to higher peak frequency. In 2008, Nieppola et al. investigated the correlation between peak

Table 1. Sample of Fermi blazars with Doppler Factors

3FGL name	Other name	redshift	Class	$\log \nu_p$	$\log L_p$	$\log L_b$	$\log L_R$	$\log L_O$	$\log L_X$	$\log L_\gamma$	δ_R	Ref
3FGL J0050.6-0929	PKS 0048-09	0.635	IBL	14.60	45.99	46.46	43.05	45.75	45.30	46.04	9.6	H09
3FGL J0108.7+0134	4C +01.02	2.099	IF	13.53	46.47	47.00	44.57	46.29	45.47	47.66	18.2	S10
3FGL J0112.1+2245	S2 0109+22	0.265	IBL	14.39	45.40	45.73	41.94	45.36	44.53	45.41	9.1	S10
3FGL J0137.0+4752	OC 457	0.859	LF	12.69	46.14	46.41	43.47	45.50	45.05	46.55	20.5	S10
3FGL J0151.6+2205	PKS 0149+21	1.320	LF	13.14	46.09	46.48	43.80	45.59		46.23	4.72	LV99
.....
.....
.....
.....

Note to the Table: Col. (1) gives the 3FGL name; Col. (2) Other name; Col. (3) redshift from NED database at IPAC; Col. (4) the SED classification by our method (Fan et al. 2016a) B stands for BL Lac, F for FSRQ, BCU for unidentified source; Col. (5) peak frequency, $\log \nu_p$ (Hz); Col. (6) peak luminosity, $\log L_p$ (erg/s); Col. (7) bolometric luminosity, $\log L_{bol}$ (erg/s); Col. (8) radio luminosity, $\log L_R$ (erg/s); Col. (9) optical luminosity, $\log L_O$ (erg/s); Col. (10) X-ray luminosity, $\log L_X$ (erg/s); Col. (11) γ -ray luminosity, $\log L_\gamma$ (erg/s); Col. (12) Doppler factor, δ_R ; and Col. (13) reference for Doppler factor. F09: Fan et al. (2009); H09: Hovatta et al. (2009); LV99: Lähteenimäki & Valtaoja (1999); S10: Savolainen et al. (2010)

Table 2. Linear Correlation Fitting Results, $y = a + bx$

$y \sim x$	$a \sim \Delta a$	$b \sim \Delta b$	N	r	p
$\log L_p^{ob} \sim \log \delta$	44.656 ± 0.178	1.330 ± 0.181	86	0.625	1.22×10^{-10}
$\log L_R^{ob} \sim \log \delta$	41.963 ± 0.209	1.484 ± 0.212	86	0.606	6.14×10^{-10}
$\log L_o^{ob} \sim \log \delta$	44.775 ± 0.190	0.935 ± 0.193	86	0.468	5.62×10^{-6}
$\log L_X^{ob} \sim \log \delta$	43.456 ± 0.239	1.521 ± 0.242	82	0.575	1.60×10^{-8}
$\log L_\gamma^{ob} \sim \log \delta$	44.304 ± 0.252	1.832 ± 0.257	86	0.614	3.15×10^{-10}
$\log L_p^{3in} \sim \log L_\gamma^{3in}$	18.472 ± 1.603	0.586 ± 0.038	86	0.858	4.49×10^{-26}
$\log L_R^{3in} \sim \log L_\gamma^{3in}$	16.675 ± 1.561	0.570 ± 0.037	86	0.858	4.86×10^{-26}
$\log L_O^{3in} \sim \log L_\gamma^{3in}$	11.650 ± 3.399	0.725 ± 0.081	86	0.699	7.36×10^{-14}
$\log L_X^{3in} \sim \log L_\gamma^{3in}$	11.591 ± 2.752	0.710 ± 0.066	82	0.771	2.43×10^{-17}
$\log L_{bol}^{3in} \sim \log L_\gamma^{3in}$	18.698 ± 1.572	0.590 ± 0.037	86	0.864	8.03×10^{-27}
$\log L_p^{4in} \sim \log L_\gamma^{4in}$	14.822 ± 1.314	0.665 ± 0.032	86	0.915	6.91×10^{-35}
$\log L_R^{4in} \sim \log L_\gamma^{4in}$	13.049 ± 1.261	0.648 ± 0.031	86	0.917	2.35×10^{-35}
$\log L_O^{4in} \sim \log L_\gamma^{4in}$	7.134 ± 2.806	0.829 ± 0.068	86	0.798	3.68×10^{-20}
$\log L_X^{4in} \sim \log L_\gamma^{4in}$	8.452 ± 2.242	0.780 ± 0.055	82	0.847	1.04×10^{-23}
$\log L_{bol}^{4in} \sim \log L_\gamma^{4in}$	15.052 ± 1.293	0.670 ± 0.031	86	0.918	1.39×10^{-35}
$\log L_p^{ob} \sim \log \nu_p^{ob}$	49.986 ± 1.678	-0.300 ± 0.122	86	-0.259	1.6%
$\log L_R^{ob} \sim \log \nu_p^{ob}$	51.138 ± 1.808	-0.571 ± 0.132	86	-0.427	4.15×10^{-5}
$\log L_O^{ob} \sim \log \nu_p^{ob}$	45.921 ± 1.633	-0.021 ± 0.119	86	-0.019	86%
$\log L_X^{ob} \sim \log \nu_p^{ob}$	49.027 ± 2.197	-0.304 ± 0.160	82	-0.208	6.1%
$\log L_\gamma^{ob} \sim \log \nu_p^{ob}$	53.918 ± 2.276	-0.580 ± 0.166	86	-0.356	7.73×10^{-4}
$\log L_p^{3in} \sim \log \nu_p^{3in}$	37.472 ± 1.081	0.451 ± 0.087	86	0.492	1.53×10^{-6}
$\log L_R^{3in} \sim \log \nu_p^{3in}$	36.971 ± 1.141	0.292 ± 0.092	86	0.327	2.13×10^{-3}
$\log L_O^{3in} \sim \log \nu_p^{3in}$	29.299 ± 1.268	1.033 ± 0.102	86	0.740	3.71×10^{-16}
$\log L_X^{3in} \sim \log \nu_p^{3in}$	34.302 ± 1.496	0.571 ± 0.121	82	0.468	9.31×10^{-6}
$\log L_\gamma^{3in} \sim \log \nu_p^{3in}$	33.734 ± 1.581	0.666 ± 0.128	86	0.495	1.26×10^{-6}
$\log L_p^{4in} \sim \log \nu_p^{4in}$	33.228 ± 1.285	0.720 ± 0.104	86	0.604	7.26×10^{-10}
$\log L_R^{4in} \sim \log \nu_p^{4in}$	32.727 ± 1.372	0.561 ± 0.111	86	0.484	2.33×10^{-6}
$\log L_O^{4in} \sim \log \nu_p^{4in}$	25.056 ± 1.485	1.302 ± 0.120	86	0.765	1.07×10^{-17}
$\log L_X^{4in} \sim \log \nu_p^{4in}$	30.024 ± 1.704	0.842 ± 0.137	82	0.566	3.08×10^{-8}
$\log L_\gamma^{4in} \sim \log \nu_p^{4in}$	29.490 ± 1.822	0.935 ± 0.147	86	0.570	9.94×10^{-10}

Note to the Table: Col. (1) gives relation. Here *3in* stands for the case of $p = 2 + \alpha$, and *4in* for $p = 3 + \alpha$; Col. (2) intercept and the corresponding uncertainty; Col. (3) slope and the corresponding uncertainty; Col. (4) number of the sample; Col. (5) correlation coefficient; and Col. (6) chance probability.

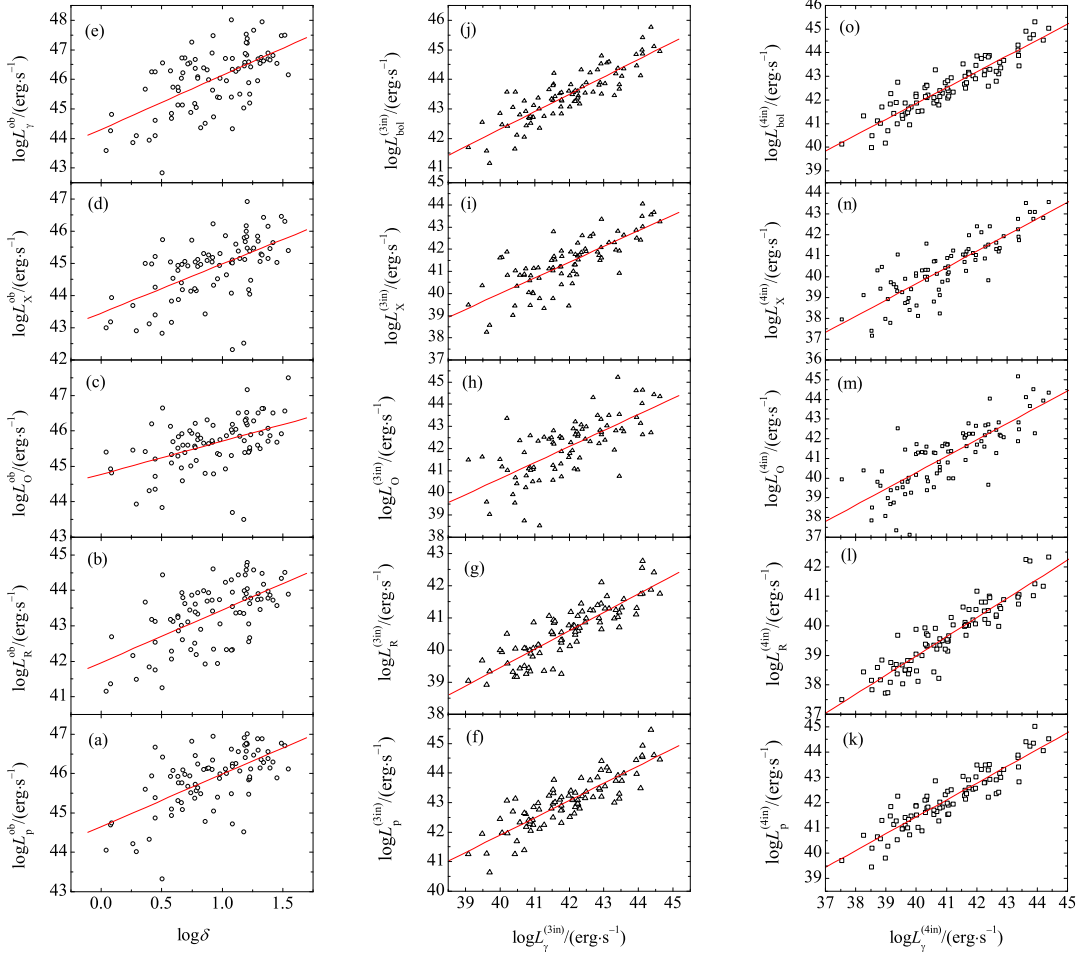


Fig. 1.— Left panel: The correlation between luminosity ($\log \nu L_{\nu}$) and peak frequency ($\log \nu_p$). From the top to the bottom is for γ -ray, X-ray, optical, radio, and peak luminosity; Middle panel: Correlation for intrinsic values between γ -ray and monochromatic luminosity for the case of $p = 2 + \alpha$ (from the top to the bottom is for bolometric, X-ray, optical, radio, and peak luminosity), and Right panel: Correlation for intrinsic values between γ -ray and monochromatic luminosity for $p = 3 + \alpha$.

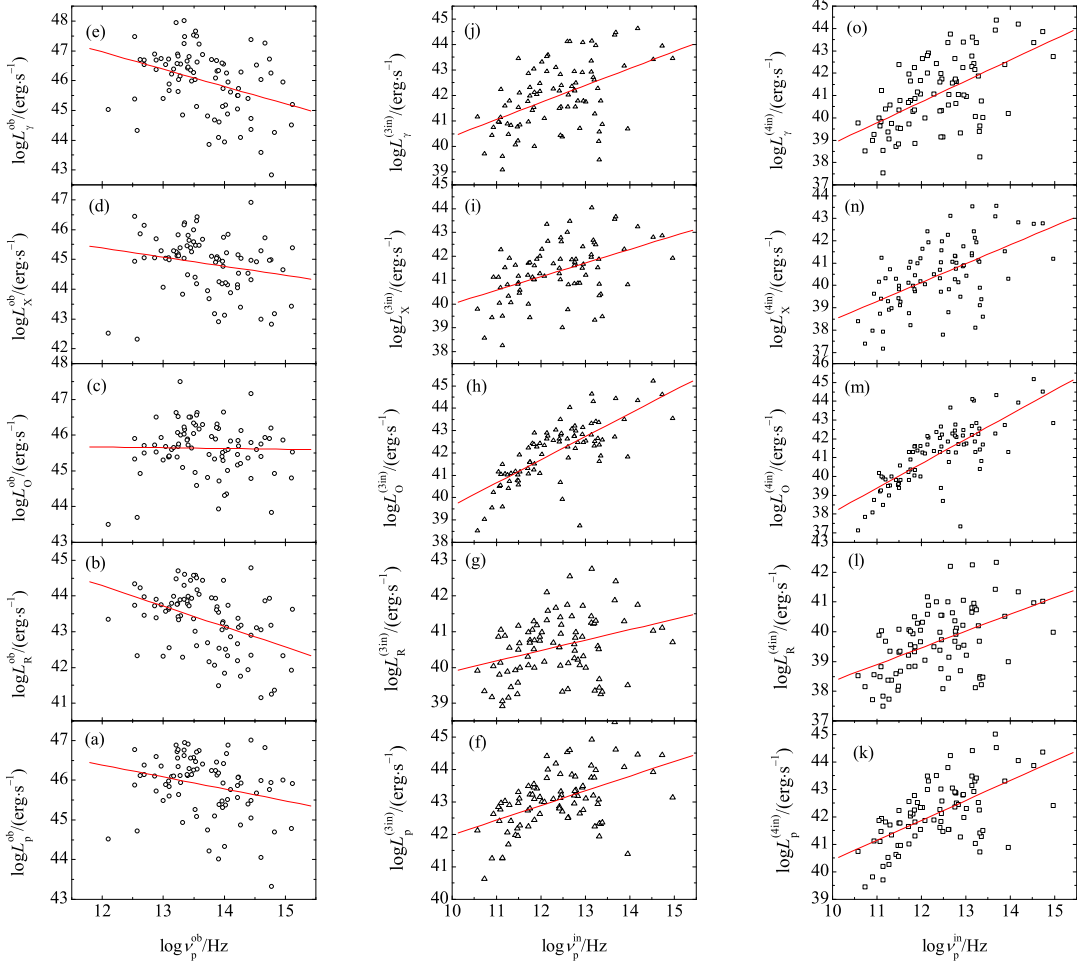


Fig. 2.— The correlation between luminosity ($\log L_\nu$) and peak frequency ($\log \nu_p$). From the upper one to the bottom one is for γ -ray, X-ray, optical, radio, and peak luminosities. Left panel: observed values, Middle panel: intrinsic values for the case of $p = 2 + \alpha$, Right panel: intrinsic values for the case of $p = 3 + \alpha$.

frequency and peak luminosity from observed and intrinsic data. The anti-correlation from the observed data was not found in the intrinsic data. Giommi et al. (2012a,b) pointed out that the anti-correlation is due to a selection effect. Their FSRQs sample was not showing any anti-correlation (Giommi et al. 2012a), while a simulation produced an anti-correlation between the radio luminosity and synchrotron peak frequency (Giommi et al. 2012b). Mao et al. (2016) calculated SEDs for a large sample of blazars from the Roma-BZCAT catalog, and found that the peak frequency increases when the radio (and bolometric) luminosity decreases.

In the present *Letter*, we compile a sample of Fermi blazars with available Doppler factors and investigate the relationship between peak luminosity (monochromatic luminosity) and Doppler factor, and that between luminosity and peak frequency. It is found that the monochromatic luminosity is closely correlated with Doppler factor, which confirms that the emissions in blazars are strongly beamed. For the correlation between luminosity and peak frequency, a close anti-correlation is found for radio luminosity, which is consistent with the results for the observed radio luminosity in Fossati et al. (1998) and Mao et al. (2016). Our result for the observed peak luminosity and peak frequency is consistent with that in Fossati et al. (1998) and Nieppola et al. (2008). It is also found that an anti-correlation exists for the γ -ray band ($r = -0.356$ and $p = 7.73 \times 10^{-4}$). But there is no correlation for optical band ($p = 86\%$), the reason is perhaps that some host galaxies in BL Lacs contribute optical emission and that the accretion disk in FSRQs contributes optical emission, which dilute the anti-correlation. When intrinsic data are considered, we have positive correlations between monochromatic (and peak) luminosity and peak frequency. Our results confirm that found in Nieppola et al. (2008) for peak luminosity and peak frequency, and show a positive correlation for the γ -ray luminosity and peak frequency as shown in Fig. 1 and Table 2. From Table 2, it can be clearly seen that the correlation coefficients for the correlations of γ -ray against the lower monochromatic luminosity (radio, optical, X-ray) and the peak luminosity in the case of $p = 3 + \alpha$ are greater than those for the corresponding correlations in the case of $p = 2 + \alpha$, and the chance probability for the correlation in the case $p = 3 + \alpha$ is much lower than that in the case of $p = 2 + \alpha$. When we consider the correlation between intrinsic luminosity and peak frequency, similar results are obtained. So, it is concluded that correlations for the intrinsic data in the case of $p = 3 + \alpha$ are closer than those in the case of $p = 2 + \alpha$ suggesting that our discussion favors a spherical jet.

For the above discussions, we use the averaged values to replace the unknown optical and X-ray spectral indexes. These replacements may cause some errors in correlation analysis. Thus, we re-investigate the correlations only for the sources with available spectral indexes, and it is found that the fitting slopes, the correlation coefficient and the chance probability introduce only little change.

Analyzing the behavior of the luminosity versus the peak frequency, we find anti-correlations in the observer frame and positive ones in intrinsic data, suggesting that the anti-correlation may arise from a beaming effect or, as discussed in the works by Giommi et al. (2012a,b), from a selection effect. In fact the sample is relatively small, as we considered here only sources which underwent flaring episodes, needed to estimate the Doppler factors, making up thus a sample of less than 10% of Fermi blazars. In our previous paper (Fan et al. 2016a), we calculated spectral energy distributions (SEDs) for 1392 Fermi blazars, out of which 999 have redshifts and only 86 have available Doppler factors, we calculate their average monochromatic luminosity at radio, optical, X-ray, and γ -ray bands, and have $\langle \log L_R \text{ (erg/s)} \rangle = 42.28 \pm 1.26$, $\langle \log L_O \text{ (erg/s)} \rangle = 45.24 \pm 0.84$, $\langle \log L_X \text{ (erg/s)} \rangle = 44.60 \pm 0.99$, and $\langle \log L_\gamma \text{ (erg/s)} \rangle = 45.27 \pm 1.31$ for the 913 sources without Doppler factors and $\langle \log L_R \text{ (erg/s)} \rangle = 43.32 \pm 0.87$, $\langle \log L_O \text{ (erg/s)} \rangle = 45.63 \pm 0.72$, $\langle \log L_X \text{ (erg/s)} \rangle = 44.86 \pm 0.96$, and $\langle \log L_\gamma \text{ (erg/s)} \rangle = 45.98 \pm 1.07$ for the 86 sources with available Doppler factors. When a K-S test is adopted to the luminosity distributions of the sources with/without known Doppler factors, it is found that the chance probability for the two luminosity distributions to be from the same distribution is $p = 4.11 \times 10^{-9}$, 1.60×10^{-6} , 1.11×10^{-3} , and 1.93×10^{-4} for their radio, optical, X-ray and γ -ray bands respectively. It indicates that the sources in our sample is obviously brighter than those without Doppler factors. So, for the sources with flaring events, their anti-correlation between observed luminosity and the peak frequency is an apparent result, their intrinsic correlation is positive. Since our Fermi blazar sample with known Doppler factor is small, we will try to compute more Doppler factors for the Fermi blazars, and re-do the analysis in the future.

In our previous work, we found that γ -ray luminosity is closely correlated with other monochromatic luminosity (X-ray, optical, and radio bands), bolometric and peak luminosity for a sample of 1392 Fermi blazars. When the redshift effect is removed, the correlation still exists between γ -ray and optical, radio, peak, and bolometric luminosities (Fan et al. 2016a). When the intrinsic luminosities are used for the correlation analysis, it is found that there are strong correlations between γ -ray luminosity and other monochromatic and peak luminosities. As listed in Table 2, we can see that strong correlations exist between γ -ray luminosity and peak, radio, and bolometric luminosities for the case of $p = 3 + \alpha$, with $r \sim 0.92$ and $p \leq 6.91 \times 10^{-35}$. We conclude by noting that strong correlations are consistent with the fact that GeV γ -rays are from SSC process in blazars.

4. Conclusions

In this *Letter*, we consider a sample of 86 flaring blazars, detected by Fermi, with available Doppler factors, calculate their intrinsic SEDs, and investigate some correlations. Our conclusions are as follows: 1) The anti-correlation between luminosity and peak frequency for the flaring sources with known Doppler factors in the observer's frame maybe caused by a beaming effect; 2) There is a positive correlation between intrinsic monochromatic (γ -ray, X-ray, optical, and radio band) luminosity and peak frequency; 3) There are strong correlations between intrinsic γ -ray and other luminosity suggesting that the GeV γ -rays are mainly from SSC; 4) Our analysis favors a spherical jet in the Fermi blazars.

The authors thank the anonymous referee for the suggestions and comments. This work is supported by the National Natural Science Foundation of China (U1531245, U1431112, 11203007, 11403006, 10633010, 11173009, 11503004), and the Innovation Foundation of Guangzhou University (IFGZ), Guangdong Innovation Group for Astrophysics(2014KCXTD014), Guangdong Province Universities and Colleges Pearl River Scholar Funded Scheme(GDUPS)(2009), Yangcheng Scholar Funded Scheme(10A027S), and supported for Astrophysics Key Subjects of Guangdong Province and Guangzhou City. This paper is dedicated to Prof. Guangzhong Xie (G.Z. Xie) who passed away on 2016 August 19 in Kunming, China.

REFERENCES

- Abdo, A. A., Ackermann, M., Atwood, W. B., et al., 2009, *ApJ*, 697, 934
- Abdo, A. A., Ackermann, M., Agudo, I., et al., 2010, *ApJ*, 716, 30
- Acerro, F., Ackermann, M., Ajello, M., et al., 2015, *ApJS*, 218, 23
- Ackermann, M., Ajello, M., Atwood, W. B., et al., 2015, *ApJ*, 810, 14
- Cheng, K. S., Fan, J. H., Zhang, L., 1999, *A&A*, 352, 32
- Cheng, K. S., Zhang, X., Zhang, L., 2000, *ApJ*, 537, 80
- Dondi, L., & Ghisellini, G., 1995, *MNRAS*, 273, 583
- Fan, J. H., Adam, G., Xie, G. Z., et al., 1998, *A&A*, 338, 27
- Fan, J. H., Xie, G. Z., Bacon, R. 1999, *A&AS*, 136, 13
- Fan, J. H., 2005, *A&A*, 436, 799

- Fan, J. H., Huang, Y., He, T. M., et al., 2009, PASJ, 61, 639
- Fan, J. H., Yang, J. H., Yuan, Y. H., et al., 2012, ApJ, 761, 125
- Fan, J. H., Yang, J. H., Liu, Y., Zhang, J.Y., 2013, RAA, 13, 259
- Fan, J. H., Bastieri, D., Yang, J. H., et al., 2014, RAA, 14, 1135
- Fan, J. H., Yang, J. H., Liu, Y., et al., 2016a, ApJS, 226, 20(arXiv:1608.03958)
- Fan, J. H., Yang, J. H., Liu, Y., et al., 2016b, JASS, 33, 105
- Fan, J. H., Yang, J. H., Liu, Y., et al., 2016c, Galaxies, 4, 16; doi:10.3390/galaxies4030016
- Fossati, G., Maraschi, L., Celotti, A., et al., 1998, MNRAS, 299, 433
- Ghisellini, G., Padovani, P., Celotti, A., Maraschi, L., 1993, ApJ, 407, 65
- Giommi, P., Polenta, G., Lähteenmäki, A., Thompson, D.J., Capalbi, M., Cutini, S., Gasparri, D., González-Nuevo, J., et al., 2012a, A&A, 541A, 160
- Giommi, P., Padovani, P., Polenta, G., Turriziani, S., DElia1, V., & Piranomonte, S., 2012b, MNRAS, 420, 2899
- Hartman, R. C., Bertsch, D. L., Bloom, S. D., et al., 1999, ApJS, 123, 79
- Hovatta, T., Valtaoja, E., Tornikorski, M., et al., 2009, A&A, 496, 527
- Huang, L. H., Jiang, D. R., & Cao, X., 1999, A&A, 341, 74
- Lähteenmäki, A., & Valtaoja, E., 1999, ApJ, 521, 493
- Lister, M. L., Cohen, M.H., Homan, D.C., et al., 2009, AJ, 138, 1874
- Mao, Peiyuan, Urry, C. M., Massaro, F., Paggi, A., Cauteruccio, J., and Künzels, S.R., 2016, ApJS, 224, 26
- Massaro, E., Maselli, A., Leto, C., et al., 2015, ApSS, 357, 75
- Mattox, J. R., Bertsch, D. L., Chiang, J., et al., 1993, ApJ, 410, 609
- Nieppola, M., Tornikoski, E., Valtaoja, E., et al., 2006, A&A, 445, 441
- Nieppola, M., Valtaoja, E., Tornikoski, E., et al., 2008 A&A, 488, 876
- Nolan, P. L., Abdo, A. A., Ackermann, M., et al., 2012, ApJS, 199, 31

Padovani, P., & Giommi, P., 1995, *ApJ*, 444, 567

Savolainen, T., Homan, D. C., Hovatta, T., et al., 2010, *A&A*, 512A, 24

von Montigny, C., Bertsch, D.L., Chiang, J., et al., 1995, *ApJ*, 440, 525

Xie, G. Z., Zhang, Y. H., Fan, J. H., 1997, *ApJ*, 477, 114

Table 3. Sample of Fermi blazars with Doppler Factors

3FGL name	Other name	redshift	Class	$\log \nu_p$	$\log L_p$	$\log L_b$	$\log L_R$	$\log L_O$	$\log L_X$	$\log L_\gamma$	δ_R	Ref
3FGL J0050.6-0929	PKS 0048-09	0.635	IBL	14.60	45.99	46.46	43.05	45.75	45.30	46.04	9.6	H09
3FGL J0112.1+2245	S2 0109+22	0.265	IBL	14.39	45.40	45.73	41.94	45.36	44.53	45.41	9.1	S10
3FGL J0222.6+4301	3C 66A	0.444	IBL	14.76	45.94	46.39	43.18	46.21	44.98	46.26	2.6	H09
3FGL J0238.6+1636	AO 0235+164	0.940	LBL	13.24	46.55	46.82	43.78	46.08	45.15	46.89	23.8	S10
3FGL J0303.6+4716	4C +47.08	0.475	IBL	14.10	45.77	46.17	42.86	45.83	43.87	45.62	4.33	F09
3FGL J0424.7+0035	PKS 0422+00	0.310	IBL	14.22	45.57	45.94	42.19	45.16	44.15	45.04	6.11	F09
3FGL J0721.9+7120	S5 0716+71	0.300	IBL	14.96	46.00	46.39	42.32	45.86	44.64	45.95	10.8	S10
3FGL J0738.1+1741	PKS 0735+17	0.424	IBL	14.23	46.07	46.45	43.13	45.69	44.53	45.74	3.92	F09
3FGL J0757.0+0956	PKS 0754+100	0.266	IBL	14.05	45.51	45.86	42.34	45.01	44.14	44.88	5.5	S10
3FGL J0811.3+0146	OJ 014	1.148	LBL	13.28	45.94	46.31	43.44	46.00		46.56	5.39	F09
3FGL J0818.2+4223	S4 0814+42	0.530	IBL	13.52	45.26	45.72	43.02	44.95	44.39	46.03	4.6	S10
3FGL J0820.9-1258	PKS 0818-128	0.074	IBL	14.77	43.33	43.93	41.25	43.83	42.83	42.84	3.18	F09
3FGL J0831.9+0430	PKS 0829+046	0.174	IBL	13.84	45.10	45.41	42.06	45.33	43.17	44.68	3.8	F09
3FGL J0854.8+2006	OJ 287	0.306	IBL	14.21	45.87	46.25	42.66	45.45	44.04	45.49	16.8	S10
3FGL J0958.6+6534	S4 0954+65	0.368	IBL	14.02	45.38	45.77	42.51	45.57	44.22	45.18	5.93	F09
3FGL J1058.5+0133	4C +01.28	0.890	IBL	13.79	46.24	46.73	43.95	45.96	45.10	46.71	12.1	S10
3FGL J1221.4+2814	W Comae	0.103	IBL	14.83	44.70	45.09	41.37	44.93	43.18	44.27	1.2	H09
3FGL J1309.5+1154	4C +12.46	0.415	IBL	13.72	44.74	45.26	42.69	44.82	43.94	44.82	1.22	F09
3FGL J1419.9+5425	OQ 530	0.153	IBL	14.27	44.87	45.25	41.75	45.21	43.40	44.10	2.79	F09
3FGL J1540.8+1449	4C +14.60	0.605	IBL	13.97	45.32	45.88	43.24	45.52	44.93	45.13	4.3	S10
3FGL J1719.2+1744	PKS 1717+177	0.137	IBL	13.91	44.02	44.45	41.49	43.93	42.91	44.09	1.94	F09
3FGL J1748.6+7005	S4 1749+70	0.770	IBL	14.27	45.93	46.39	43.18	46.13	45.04	46.28	3.75	F09
3FGL J1751.5+0939	OT 081	0.322	LBL	12.99	45.50	45.76	42.32	45.30	44.07	45.40	11.9	S10
3FGL J1800.5+7827	S5 1803+784	0.680	IBL	13.90	46.18	46.59	43.55	46.19	45.01	46.33	12.1	S10
3FGL J1806.7+6949	3C 371	0.051	IBL	14.60	44.05	44.51	41.16	45.40	42.99	43.58	1.1	S10
3FGL J1824.2+5649	4C +56.27	0.664	LBL	13.25	45.64	46.04	43.33	45.75	45.12	46.03	6.3	S10
3FGL J2005.2+7752	S5 2007+77	0.342	IBL	13.55	45.08	45.49	42.61	44.60	44.18	45.14	4.68	F09
3FGL J2134.1-0152	PKS 2131-021	1.283	LBL	13.17	46.10	46.55	43.99	45.65	45.30	46.38	7	F09
3FGL J2202.7+4217	BL Lacertae	0.069	IBL	15.10	44.78	45.24	41.92	44.80	43.44	44.52	7.2	S10
3FGL J2236.3+2829	B2 2234+28A	0.795	LBL	12.88	45.73	46.02	43.39	45.52		46.37	6	H09
3FGL J0108.7+0134	4C +01.02	2.099	IF	13.53	46.47	47.00	44.57	46.29	45.47	47.66	18.2	S10
3FGL J0137.0+4752	OC 457	0.859	LF	12.69	46.14	46.41	43.47	45.50	45.05	46.55	20.5	S10
3FGL J0151.6+2205	PKS 0149+21	1.320	LF	13.14	46.09	46.48	43.80	45.59		46.23	4.72	LV99
3FGL J0217.5+7349	S5 0212+73	2.367	LF	13.35	46.95	47.31	44.60	46.15	46.23	47.47	8.4	S10
3FGL J0217.8+0143	PKS 0215+015	1.715	IF	14.66	46.83	47.27	43.87	45.93	45.72	47.26	5.61	F09

Table 3—Continued

3FGL name	Other name	redshift	Class	$\log \nu_p$	$\log L_p$	$\log L_b$	$\log L_R$	$\log L_O$	$\log L_X$	$\log L_\gamma$	δ_R	Ref
3FGL J0237.9+2848	4C +28.07	1.213	IF	13.59	46.75	47.10	44.05	46.17	45.47	47.23	16	S10
3FGL J0309.0+1029	PKS 0306+102	0.863	IF	14.04	46.68	46.96	43.12	44.36	45.21	46.25	2.79	F09
3FGL J0336.5+3210	NRAO 140	1.259	IF	13.55	46.28	46.72	44.17	46.63	46.43	46.62	22	S10
3FGL J0339.5-0146	PKS 0336-01	0.850	LF	13.40	46.12	46.51	43.79	45.89	44.48	46.42	17.2	S10
3FGL J0423.2-0119	PKS 0420-01	0.916	LF	12.88	46.60	46.84	43.90	46.51	45.69	46.70	19.7	S10
3FGL J0449.0+1121	PKS 0446+11	1.207	LF	13.09	45.98	46.35	43.63	45.39	45.06	46.72	4.9	LV99
3FGL J0501.2-0157	S3 0458-02	2.286	LF	13.50	46.57	47.03	44.58	46.33	45.99	47.53	15.7	S10
3FGL J0530.8+1330	PKS 0528+134	2.070	LF	12.53	46.78	47.03	44.34	45.91	46.45	47.47	30.9	S10
3FGL J0608.0-0835	PKS 0605-08	0.872	IF	13.88	46.13	46.58	43.70	46.31	45.09	46.32	7.5	S10
3FGL J0739.4+0137	PKS 0736+01	0.189	IF	14.43	45.04	45.51	42.34	44.78	44.32	44.73	8.5	S10
3FGL J0807.9+4946	OJ 508	1.434	LF	13.28	46.12	46.50	43.90	47.49	45.39	46.15	35.2	S10
3FGL J0830.7+2408	OJ 248	0.939	LF	13.50	46.26	46.59	43.36	46.04	45.60	46.27	13	S10
3FGL J0841.4+7053	S5 0836+71	2.218	IF	14.44	47.01	47.53	44.78	47.16	46.91	47.39	16.1	S10
3FGL J0850.2-1214	PMN J0850-1213	0.566	LF	13.10	45.84	46.02	42.55	45.40		45.89	16.5	H09
3FGL J0948.6+4041	4C +40.24	1.249	IF	13.86	46.25	46.72	43.94	45.90	44.90	46.08	6.3	S10
3FGL J0956.6+2515	OK 290	0.708	IF	13.98	45.93	46.34	43.27	45.29	44.77	45.74	4.3	H09
3FGL J0957.6+5523	4C +55.17	0.899	IF	14.74	45.76	46.40	43.94	45.91	44.97	46.73	4.63	LV99
3FGL J1037.0-2934	PKS 1034-293	0.312	IF	13.92	45.39	45.78	42.55	44.71	44.25	44.61	2.8	F09
3FGL J1129.9-1446	PKS 1127-14	1.184	IF	13.99	46.42	46.93	44.44	46.65	45.73	46.56	3.22	F09
3FGL J1159.5+2914	Ton 599	0.725	LF	13.04	45.89	46.29	43.57	45.68	45.03	46.54	28.2	S10
3FGL J1224.9+2122	4C +21.35	0.432	IF	14.53	45.68	46.16	43.12	45.60	44.92	46.52	5.2	S10
3FGL J1229.1+0202	3C 273	0.158	IF	15.12	45.92	46.52	43.63	45.53	45.38	45.20	16.8	S10
3FGL J1256.1-0547	3C 279	0.536	LF	12.69	46.39	46.76	43.98	45.71	46.15	46.68	23.8	S10
3FGL J1310.6+3222	OP 313	0.998	LF	13.22	46.72	47.03	43.77	45.39	45.12	46.57	15.3	S10
3FGL J1326.8+2211	B2 1324+22	1.400	LF	12.97	46.35	46.70	43.76	45.94	45.29	46.74	21	S10
3FGL J1337.6-1257	PKS 1335-127	0.539	LF	13.25	46.34	46.68	43.42	45.69	45.18	45.64	8.3	S10
3FGL J1408.8-0751	PKS B1406-076	1.494	LF	12.86	46.11	46.43	43.72	45.72	45.05	46.88	8.26	LV99
3FGL J1504.4+1029	PKS 1502+106	1.838	LF	13.34	46.62	47.00	44.30	46.03	45.03	48.01	11.9	S10
3FGL J1512.8-0906	PKS 1510-08	0.360	IF	13.97	45.47	45.94	43.06	45.40	44.18	46.59	16.5	S10
3FGL J1608.6+1029	4C +10.45	1.226	LF	13.39	46.15	46.59	43.86	45.87	45.46	46.66	24.8	S10
3FGL J1613.8+3410	OS 319	1.399	LF	13.44	46.56	46.98	44.43	46.51	45.38	46.35	13.6	S10
3FGL J1635.2+3809	4C +38.41	1.813	LF	13.21	46.88	47.24	44.48	46.63	45.25	47.94	21.3	S10
3FGL J1637.9+5719	OS 562	0.751	IF	14.22	46.07	46.53	43.37	45.85	45.16	45.50	13.9	S10
3FGL J1642.9+3950	3C 345	0.593	LF	13.46	46.15	46.61	43.93	45.64	45.26	45.99	7.7	S10
3FGL J1728.5+0428	PKS 1725+044	0.296	LF	13.32	44.94	45.25	42.29	45.10	43.83	44.84	3.8	H09

Table 3—Continued

3FGL name	Other name	redshift	Class	$\log \nu_p$	$\log L_p$	$\log L_b$	$\log L_R$	$\log L_O$	$\log L_X$	$\log L_\gamma$	δ_R	Ref
3FGL J1733.0-1305	PKS 1730-13	0.902	LF	12.62	46.12	46.51	44.23	44.93	45.86	46.70	10.6	S10
3FGL J1740.3+5211	4C +51.37	1.375	LF	13.42	46.29	46.68	43.72	46.50	45.64	46.80	26.3	S10
3FGL J1744.3-0353	PKS 1741-03	1.054	IF	14.06	46.89	47.27	43.74	45.59	45.84	45.95	19.5	S10
3FGL J1924.8-2914	PKS B1921-293	0.352	LF	12.53	45.88	46.14	43.74	45.33	44.94	45.38	9.51	F09
3FGL J2123.6+0533	OX 036	1.941	LF	13.40	46.91	47.25	43.99	45.73	45.80	46.46	15.2	S10
3FGL J2147.2+0929	PKS 2144+092	1.113	IF	13.87	46.46	46.81	43.62	46.21	45.04	46.67	5.96	LV99
3FGL J2158.0-1501	PKS 2155-152	0.672	LF	13.09	45.60	46.00	43.67	45.41	44.99	45.67	2.31	F09
3FGL J2203.7+3143	4C +31.63	0.295	IF	14.43	45.48	45.96	42.91	45.79	44.96	44.37	6.6	S10
3FGL J2225.8-0454	3C 446	1.404	LF	13.24	46.77	47.20	44.70	46.52	45.83	46.83	15.9	S10
3FGL J2229.7-0833	PKS 2227-08	1.560	LF	13.34	46.76	47.09	43.91	46.23	46.16	47.24	15.8	S10
3FGL J2232.5+1143	CTA 102	1.037	IF	13.65	46.41	46.88	44.43	46.30	45.68	46.88	15.5	S10
3FGL J2254.0+1608	3C 454.3	0.859	IF	13.54	46.71	47.16	44.51	46.56	46.30	47.49	32.9	S10
3FGL J0205.0+1510	4C +15.05	0.405	LBCU	12.10	44.53	44.99	43.35	43.50	42.53	45.03	15	S10
3FGL J0522.9-3628	PKS 0521-36	0.057	IBCU	13.75	44.23	44.60	42.16	45.46	43.69	43.87	1.83	F09
3FGL J0725.8-0054	PKS 0723-008	0.128	IBCU	14.00	44.34	44.81	41.84	44.31	43.12	43.94	2.5	LV99
3FGL J1416.0+1325	PKS B1413+135	0.247	LBCU	12.57	44.73	44.97	42.32	43.70	42.33	44.34	12.1	S10

Note to the Table: Col. (1) gives the 3FGL name; Col. (2) Other name; Col. (3) redshift from NED database at IPAC; Col. (4) the SED classification by our method (Fan et al. 2016a) F stands for FSRQ, B for BL Lac; Col. (5) peak frequency, $\log \nu_p$ (Hz); Col. (6) peak luminosity, $\log L_p$ (erg/s); Col. (7) bolometric luminosity, $\log L_{bol}$ (erg/s); Col. (8) radio luminosity, $\log L_R$ (erg/s); Col. (9) optical luminosity, $\log L_O$ (erg/s); Col. (10) X-ray luminosity, $\log L_X$ (erg/s); Col. (11) γ -ray luminosity, $\log L_\gamma$ (erg/s); Col. (12) Doppler factor, δ_R ; and Col. (13) reference for Doppler factor. F09: Fan et al. (2009); H09: Hovatta et al. (2009); LV99: Lähteenimäki & Valtaoja (1999); S10: Savolainen et al. (2010)